Doubly-charged scalar in four-body decays of neutral flavored mesons*

Tian-Hong Wang(王天鸿) Geng Li(李更) Yue Jiang(姜越) Guo-Li Wang(王国利)[1)]

Department of Physics, Harbin Institute of Technology, Harbin 150001, China

Abstract: We study the four-body decays of neutral flavored mesons, including $\bar{K}^0$, D^0, $\bar{B}^0$, and $\bar{B}^0_s$. These processes, which could be induced by a hypothetical doubly-charged scalar particle, do not conserve the lepton number. Assuming, as an example, that the mass of the doubly-charged particle is 1000 GeV, and using the upper bounds of the couplings, we calculate the branching ratios of different channels. For $\bar{K}^0\to h_1^+h_2^+e^-e^-$, $D^0\to h_1^-h_2^-e^+e^+$, and $\bar{B}^0_{d,s}\to h_1^+h_2^+e^-e^-$, it is of the order of 10^{-30}, 10^{-32}–10^{-29}, and 10^{-33}–10^{-28}, respectively. Based on the experimental results for the $D^0\to h_1^-h_2^-l_1^+l_2^+$ channels, we also find the upper limit for the quantity $\frac{s_\Delta h_{ij}}{M^2_\Delta}$.

Keywords: doubly-charged scalar, four-body decay, neutral flavored meson

PACS: 12.39.Hg **DOI:** 10.1088/1674-1137/43/1/013103

1 Introduction

In a previous paper [1], we studied the lepton number violation decays of the B_c^- meson induced by a doubly-charged Higgs boson. There are both experimental and theoretical motivations to study this kind of particle. Although the Higgs boson has been found, whether it is the one predicted by the Standard Model still needs more confirmation. It is possible that an extended Higgs sector exists, and that there are additional isospin multiplet scalar fields. For example, the $SU(2)_{\rm L}$ triplet scalar, which contains a doubly-charged component, is introduced to generate small neutrino mass in the Type-II seesaw modes [2–5]. Generally, such a triplet representation is needed in the left-right symmetric models [6–8] to break the extended $SU(2)_{\rm L}\times SU(2)_{\rm R}\times U(1)_{B-L}$ symmetry in the Standard Model. The doubly-charged scalar also appears in other models, such as little Higgs models [9] and Georgi-Machacek model [10]. As it can decay into two leptons with the same charge, indicating lepton number violation, such processes for top quark, τ^- [11], and charged mesons, such as K^-, D^-, D_s^-, B^- [12–15] have been investigated extensively. As the lower bound of the mass of the doubly-doubly charged Higgs boson is around 800 GeV [16, 17], these low energy processes have extremely small branching ratios. Although it is not likely that these channels will be detected soon, as experiments collect more data, the upper limits of the branching ratios for such decay processes will become more stringent. One can also use them to derive further constraints for the effective short-range interactions [18].

In Ref. [1], we considered both the three-body and four-body decay channels of B_c^- meson, in which the lepton number is not conserved. In this paper, we investigate the lepton number violation processes of the neutral flavored mesons induced by the doubly-charged Higgs boson. Contrary to the charged meson case, where the annihilation-type diagram and the two W meson emitting diagram both contribute to the amplitude, in the case of the neutral meson, the light antiquark is just a spectator (see Fig. 1). Theoretically, this makes the calculation simpler, as there is no complexity brought by the cascade decay. As for the decay products, the two leptons have the same charge, and so do the two mesons. These decay modes have no equivalent in the Standard Model, which makes them also interesting experimentally.

These channels can also be induced by Majorana-type neutrinos. Their Feynman diagrams are similar to Fig. 1, but the s channels should be replaced by t channels. If the neutrino mass were around GeV, it could be produced on-shell, which has attracted much attention [19–22]. For the cases when the neutrino mass is very small or very large, the branching ratios will have the same order of magnitude as in the case of the doubly-charged Higgs boson [15, 23]. Therefore, the theoretical analy-

Received 20 July 2018, Revised 10 October 2018, Published online 20 November 2018

∗ Supported by National Natural Science Foundation of China (11405037, 11575048, 11505039)

1) E-mail: gl_wang@hit.edu.cn, Corresponding author

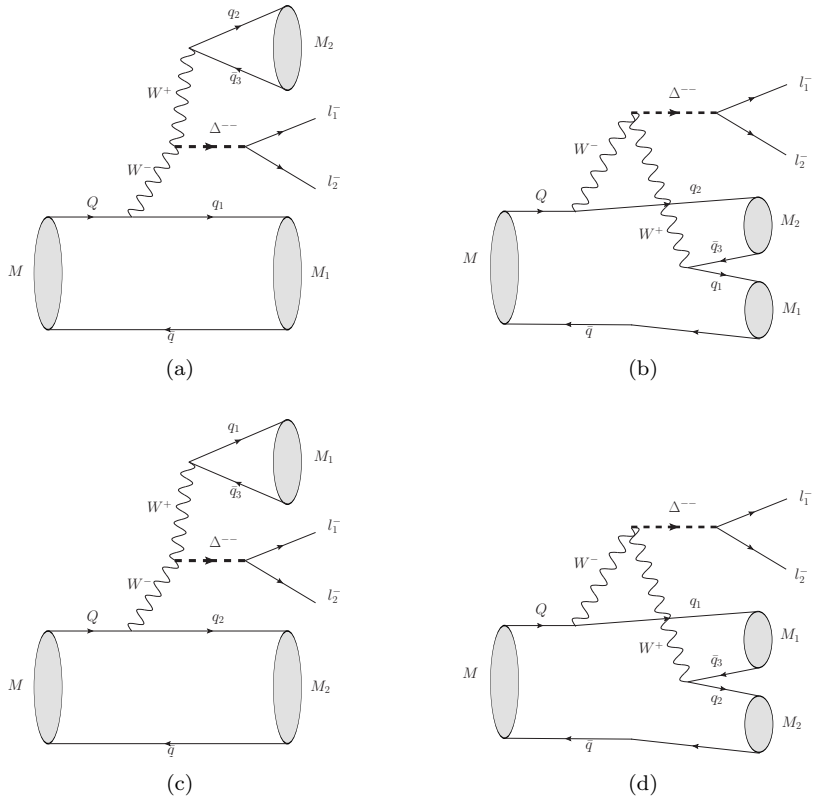

Fig. 1. Feynman diagrams of the decay processes $h\to h_1h_2l_1^-l_2^-$.

sis of the low energy processes induced by the doubly-charged Higgs boson also provides a useful complement to the Majorana neutrino scenario.

This paper is organized as follows. In Sec. 2, we give the Lagrangian which describes the couplings between the Higgs triplet and the Standard Model particles, and present the amplitudes and phase space integrals. In Sec. 3, we give the branching ratios of all decay channels and compare the results for D^0 with experimental data. We summarize our results in the last section. Some details of the meson wave functions are presented in the Appendix.

2 Theoretical formalism

The hypothetical Higgs triplet Δ in the 2×2 representation is defined as [12]

$$\Delta=\begin{pmatrix}\Delta^+/\sqrt{2} & \Delta^{++}\\ \Delta^0 & -\Delta^+/\sqrt{2}\end{pmatrix}. \tag{1}$$

It mixes with the usual $SU(2)_L$ Higgs doublet by a mixing angle θ_Δ, from which we define $s_\Delta=\sin\theta_\Delta$ and $c_\Delta=\cos\theta_\Delta$.

The Lagrangian which describes the interaction between Δ and W^- gauge boson or SM fermions has the following form [12, 15]

$$\begin{aligned}\mathcal{L}'_{\rm int}=&{\rm i}h_{ij}\psi_{iL}^TC\sigma_2\Delta\psi_{jL}-\sqrt{2}gm_Ws_\Delta\Delta^{++}W^{-\mu}W^-_\mu\\&+\frac{\sqrt{2}}{2}gc_\Delta W^{-\mu}\Delta^-\overset{\leftrightarrow}{\partial}_\mu\Delta^{++}\\&+\frac{{\rm i}gs_\Delta}{\sqrt{2}m_Wc_\Delta}\Delta^+(m_{q'}\bar{q}_Rq'_R-m_q\bar{q}_Lq'_L)+{\rm H.c.},\end{aligned} \tag{2}$$

where $C=i\gamma^2\gamma^0$ is the charge conjugation matrix; ψ_{iL} represents the leptonic doublet; h_{ij} is the leptonic Yukawa coupling constant; g is the weak coupling constant. The third and fourth terms represent the interactions between the singly-charged boson and the other particles. Compared with the second term, their contributions can be neglected.

If $q=q_3$, all four diagrams in Fig. 1 contribute to the decay:

$$\begin{aligned}\mathcal{M}_A=&\frac{g^3}{8\sqrt{2}m_W^3}V_{q_1Q}V_{q_2q_3}\frac{s_\Delta h_{ij}}{m_\Delta^2}\langle h_1(p_1)h_2(p_2)|(\bar{q}_1Q)_{V-A}(\bar{q}_2q_3)_{V-A}|h(p)\rangle\langle{\rm lepton}\rangle\\=&\frac{g^3}{8\sqrt{2}m_W^3}V_{q_1Q}V_{q_2q_3}\frac{s_\Delta h_{ij}}{m_\Delta^2}f_{h_2}p_2^\mu\langle h_1(p_1)|\bar{q}_1\gamma_\mu(1-\gamma_5)Q|h(p)\rangle\langle{\rm lepton}\rangle,\end{aligned} \tag{3}$$

$$\mathcal{M}_B=\frac{g^3}{8\sqrt{2}m_W^3}V_{q_2Q}V_{q_1q_3}\frac{s_\Delta h_{ij}}{m_\Delta^2}\langle h_1(p_1)h_2(p_2)|(\bar{q}_2Q)_{V-A}(\bar{q}_1q_3)_{V-A}|h(p)\rangle\langle\text{lepton}\rangle$$
$$=\frac{g^3}{8\sqrt{2}m_W^3}\frac{1}{3}V_{q_2Q}V_{q_1q_3}\frac{s_\Delta h_{ij}}{m_\Delta^2}f_{h_2}p_2^\mu\langle h_1(p_1)|\bar{q}_1\gamma_\mu(1-\gamma_5)Q|h(p)\rangle\langle\text{lepton}\rangle, \quad (4)$$

$$\mathcal{M}_C=\frac{g^3}{8\sqrt{2}m_W^3}V_{q_2Q}V_{q_1q_3}\frac{s_\Delta h_{ij}}{m_\Delta^2}\langle h_1(p_1)h_2(p_2)|(\bar{q}_2Q)_{V-A}(\bar{q}_1q_3)_{V-A}|h(p)\rangle\langle\text{lepton}\rangle$$
$$=\frac{g^3}{8\sqrt{2}m_W^3}V_{q_2Q}V_{q_1q_3}\frac{s_\Delta h_{ij}}{m_\Delta^2}f_{h_1}p_1^\mu\langle h_2(p_2)|\bar{q}_2\gamma_\mu(1-\gamma_5)Q|h(p)\rangle\langle\text{lepton}\rangle, \quad (5)$$

$$\mathcal{M}_D=\frac{g^3}{8\sqrt{2}m_W^3}V_{q_1Q}V_{q_2q_3}\frac{s_\Delta h_{ij}}{m_\Delta^2}\langle h_1(p_1)h_2(p_2)|(\bar{q}_1q_3)_{V-A}(\bar{q}_2Q)_{V-A}|h(p)\rangle\langle\text{lepton}\rangle$$
$$=\frac{g^3}{8\sqrt{2}m_W^3}\frac{1}{3}V_{q_1Q}V_{q_2q_3}\frac{s_\Delta h_{ij}}{m_\Delta^2}f_{h_1}p_1^\mu\langle h_2(p_2)|\bar{q}_2\gamma_\mu(1-\gamma_5)Q|h(p)\rangle\langle\text{lepton}\rangle, \quad (6)$$

where the factor $\frac{1}{3}$ in $\mathcal{M}_B$ and $\mathcal{M}_D$ is introduced by the Fierz transformation; $\langle\text{lepton}\rangle$ is the leptonic part of the transition matrix element; $V_{q_iq_j}$ is the Cabibbo-Kobayashi-Maskawa matrix element. The definition of the decay constant f_{h_1} of a pseudoscalar meson

$$\langle h_1(p_1)|\bar{q}_1\gamma^\mu(1-\gamma_5)q_2|0\rangle=\mathrm{i}f_{h_1}p_1^\mu \quad (7)$$

is used. For vector mesons, it should be replaced by

$$\langle h_1(p_1,\epsilon)|\bar{q}_1\gamma^\mu(1-\gamma_5)q_2|0\rangle=M_1f_{h_1}\epsilon^\mu. \quad (8)$$

The values of the decay constants are given in Table 1. It should be pointed out that we have used the factorization assumption in Eqs. (3)–(6), which is not quite appropriate when both final mesons are light. However, as only the order of magnitude is important in such processes, we anticipate that the effects of nonfactorization and final meson interactions do not change the results significantly.

Finally, we get the transition amplitude

$$\mathcal{M}=\mathcal{M}_A+\mathcal{M}_B+\mathcal{M}_C+\mathcal{M}_D$$
$$=\frac{g^3s_\Delta h_{ij}}{8\sqrt{2}m_W^3m_\Delta^2}\Big\{(V_{q_1Q}V_{q_2q_3}+\frac{1}{3}V_{q_2Q}V_{q_1q_3})f_{h_2}p_2^\mu$$
$$\times\langle h_1(p_1)|\bar{q}_1\gamma_\mu(1-\gamma_5)Q|h(p)\rangle$$
$$+(V_{q_2Q}V_{q_1q_3}+\frac{1}{3}V_{q_1Q}V_{q_2q_3})f_{h_1}p_1^\mu$$
$$\times\langle h_2(p_2)|\bar{q}_2\gamma_\mu(1-\gamma_5)Q|h(p)\rangle\Big\}\langle\text{lepton}\rangle. \quad (9)$$

If $q\neq q_3$, only Fig. 1(a) and (b) contribute:

$$\mathcal{M}=\mathcal{M}_A+\mathcal{M}_B$$
$$=\frac{g^3s_\Delta h_{ij}}{8\sqrt{2}m_W^3m_\Delta^2}(V_{q_1Q}V_{q_2q_3}+\frac{1}{3}V_{q_2Q}V_{q_1q_3})f_{h_2}p_2^\mu$$
$$\times\langle h_1(p_1)|\bar{q}_1\gamma_\mu(1-\gamma_5)Q|h(p)\rangle\langle\text{lepton}\rangle. \quad (10)$$

The hadronic transition matrix can be expressed as [27]

$$\langle h_1(p_1)|V^\mu|h(p)\rangle=f_+(Q^2)(p+p_1)^\mu+f_-(Q^2)(p-p_1)^\mu, \quad (11)$$

where h_1 is a pseudoscalar meson, and f_+ and f_- are form factors. If h_1 is a vector meson, we have

$$\langle h_1(p_1,\epsilon)|V^\mu|h(p)\rangle=-\mathrm{i}\frac{2}{M+M_1}f_V(Q^2)\epsilon^{\mu\epsilon^*pp_1},$$
$$\langle h_1(p_1,\epsilon)|A^\mu|h(p)\rangle=f_1(Q^2)\frac{\epsilon^*\cdot p}{M+M_1}(p+p_1)^\mu$$
$$+f_2(Q^2)\frac{\epsilon^*\cdot p}{M+M_1}(p-p_1)^\mu$$
$$+f_0(Q^2)(M+M_1)\epsilon^{*\mu}, \quad (12)$$

where f_V and f_i (i=0, 1, 2) are form factors; M and M_1 are the masses of corresponding mesons; the definition $Q=p-p_1$ is used.

By applying the Bethe-Salpeter method with the instantaneous approximation [28], the hadronic matrix element is written as

$$\langle h_1(p_1)|\bar{q}_1\gamma^\mu(1-\gamma_5)Q|h(p)\rangle$$
$$=\int\frac{\mathrm{d}^3q}{(2\pi)^3}\mathrm{Tr}\left[\frac{\not{p}}{M}\overline{\varphi^{++}_{p_1}}(\vec{q}_1)\gamma_\mu(1-\gamma_5)\varphi^{++}_p(\vec{q})\right], \quad (13)$$

where φ^{++} is the positive energy part of the wave function; $\vec{q}$ and $\vec{q}_1$ are the relative three-momenta between the quarks and antiquarks in the initial and final mesons, respectively.

Table 1. Decay constants of mesons (in MeV). The values for π, K, D, and D_s are from Particle Data Group [24]; K^* and ρ, are from Ref. [25]; D^* and D_s^* are from Ref. [26].

f_π	f_K	f_{K^*}	f_ρ	f_D	f_{D_s}	f_{D^*}	$f_{D_s^*}$
130.4	156.2	217	205	204.6	257.5	340	375

The partial decay width is obtained by evaluating the phase space integral

$$\Gamma=\left(1-\frac{1}{2}\delta_{h_1h_2}\right)\left(1-\frac{1}{2}\delta_{l_1l_2}\right)\int\frac{\mathrm{d}s_{12}}{s_{12}}\int\frac{\mathrm{d}s_{34}}{s_{34}} \times\int\mathrm{d}\cos\theta_{12}\int\mathrm{d}\cos\theta_{34}\int\mathrm{d}\phi\mathcal{K}|\mathcal{M}|^2, \tag{14}$$

where

$$\mathcal{K}=\frac{1}{2^{15}\pi^6M^3}\lambda^{1/2}(M^2,s_{12},s_{34})\lambda^{1/2}(s_{12},M_1^2,M_2^2) \times\lambda^{1/2}(s_{34},m_1^2,m_2^2). \tag{15}$$

We also use the definitions $s_{12}=(p_1+p_2)^2$ and $s_{34}=(p_3+p_4)^2$. The meanings of θ_{12}, θ_{34}, and ϕ are shown in Fig. 2. $\delta_{l_1l_2}$ is 1 if l_1 and l_2 are identical particles, otherwise it is 0. The same is true for $\delta_{h_1h_2}$. The integral limits are

$$\begin{aligned} &s_{12}\in[(M_1+M_2)^2,\ (M-m_1-m_2)^2],\\ &s_{34}\in[(m_1+m_2)^2,\ (M-\sqrt{s_{12}})^2],\\ &\phi\in[0,\ 2\pi],\quad \theta_{12}\in[0,\ \pi],\quad \theta_{34}\in[0,\ \pi], \end{aligned} \tag{16}$$

where M_2, m_1, and m_2 are the masses of h_2, l_1, and l_2, respectively.

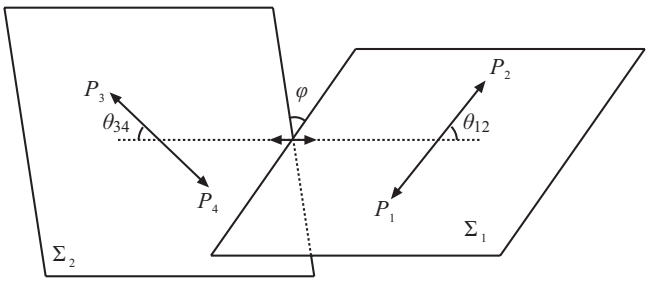

Fig. 2. Kinematics of the four-body decay of h in its rest frame. P_1 and P_2 are respectively the momenta of h_1 and h_2 in their center-of-momentum frame; P_3 and P_4 are respectively the momenta of l_1 and l_2 in their center-of-momentum frame.

3 Numerical results

The Bethe-Salpeter method has certain advantages when calculating the form factors, especially in the case when both initial and final mesons are heavy. In the first step, the wave functions of the mesons, which include relativistic corrections, are obtained by solving numerically the corresponding instantaneous Bethe-Salpeter equation. Their pole structure is important for describing the properties of heavy mesons. Subsequently, the form factors for the physically allowed region are calculated using Eq. (13) without any analytic extension. Although the instantaneous approximation is reasonable for the double heavy mesons and acceptable for the heavy-light mesons, it results in large errors for the light mesons, such as π and K. For example, when we change the parameters by $\pm5\%$, the form factors at $Q^2=0$ for the channels with heavy mesons change by less than 10%, while for those with π or K, the errors can be larger than 50%. For processes with light mesons, such as $B\to\pi(\rho)$, other methods are more appropriate, for example the light-cone sum rules. Nevertheless, we use this approximation also for the light mesons as the decay channels we consider are related to new physics, for which the branching ratios are expected to be very small, and only the order of magnitude is important.

The parameters of the doubly-charged Higgs boson have no definite values at present, only the lower or upper limits from experiments are available. For example, the latest results of the ATLAS and CMS Collaborations [16, 17] show that the mass of Δ^{++} is larger than 800 GeV. From Ref. [12], the upper limit for s_Δ is 0.0056. The constraints for the coupling h_{ee} can be extracted from the e^+e^- annihilation process [29]: $\frac{h_{ee}^2}{m_\Delta^2}\leq9.7\times10^{-6}$ GeV^{-2}. For $h_{\mu\mu}$, the Muon $g-2$ experiment provides the limit [30]: $\frac{h_{\mu\mu}^2}{m_\Delta^2}\leq3.4\times10^{-6}$ GeV^{-2}. The $h_{e\mu}$ is related to $\mu^-\to e^-e^+e^-$ and $\mu^-\to e^-\gamma$ processes [12], which give $\frac{h_{e\mu}h_{ee}}{m_\Delta^2}\leq3.2\times10^{-11}$ GeV^{-2} and $\frac{h_{e\mu}h_{\mu\mu}}{m_\Delta^2}\leq2.0\times10^{-10}$ GeV^{-2}, respectively. Taking $m_\Delta=1000$ GeV as an example, we can estimate the upper limits of the quantity $\left(\frac{s_\Delta h_{ij}}{m_\Delta^2}\right)^2$ for the ee and $\mu\mu$ cases as 3.0×10^{-16} and 1.1×10^{-16}, respectively. For the $e\mu$ case, following the method applied in Ref. [12], we let h_{ee} and $h_{\mu\mu}$ equal to their upper bound, and get $h_{e\mu}\leq1.1\times10^{-16}$, which leads to $\left(\frac{s_\Delta h_{e\mu}}{m_\Delta^2}\right)^2\leq3.3\times10^{-27}$.

For $\bar{K}^0$, there are only three channels allowed by the phase space, namely $\pi^+\pi^+l_1^-l_2^-$ $(l_i=e,\ \mu)$. The corresponding diagrams are Fig. 1(a)–(d). The $\pi^+\pi^+e^-e^-$ channel has the largest branching ratio, which is of the order of 10^{-30} (see Table 2). Experimentally, $Br(K^+\to\pi^-l_1^+l_2^+)\lesssim10^{-10}$ [31], which is the most precise result for lepton number violation. However, lepton number violation in four-body decay channels of this particle has not been experimentally found. In Refs. [32, 33], the channels $K_{L,S}\to\pi^+\pi^-e^+e^-$ are investigated. We hope that the $K_{L,S}\to\pi^+\pi^+l_1^-l_2^-$ channels will be experimentally studied in the future.

For D^0, the final mesons can be pseudoscalars or vectors. The results for the case when h_1 and h_2 are both pseudoscalars, that is $\pi\pi$, πK, or KK, are given in Table 3. The largest value is of the order of magnitude of 10^{-29}. We note that the Fermilab E791 Collaboration presented the upper limits of the branching ratios for these channels [34], which are of the order of 10^{-5}. By comparing the theoretical predictions and experimental data, we find the upper limit of the constant $\frac{s_\Delta h_{ij}}{m_\Delta^2}$ of the

order of 10^4 GeV^{-2}. One can also extract this upper limit from the three-body decay processes, such as $D^- \to \pi^+ e^- e^-$, which gives about 10^2 GeV^{-2} by using the results in Ref. [12]. The branching ratios of D^0 decay channels, where h_1 and h_2 are 0^-1^- or 1^-1^-, are given in Table 4; the largest value has the order of magnitude of 10^{-29}.

The results for $\bar{B}^0$ and $\bar{B}^0_s$ are given in Tables 5–10. The largest value is of the order of 10^{-28}. In Ref. [35], the four-body decay channel $B^- \to D^0\pi^+\mu^-\mu^-$ was measured to have a branching ratio of less than 1.5×10^{-6}. There are no experimental values available at present for the neutral B meson decay channels. However, as LHCb is continuing to run, more data will be available. We expect that the LHCb Collaboration will detect such decay modes and will set more stringent constraints on the parameters of doubly-charged Higgs boson. Besides, the future B-factories, such as Belle-II, will also have the possibility of providing more information about these channels.

Table 2. The upper limit of Br for different decay channels of $\bar{K}^0$.

decay channel	upper limit of Br
$\bar{K}^0 \to \pi^+\pi^+ e^- e^-$	2.2×10^{-30}
$\bar{K}^0 \to \pi^+\pi^+ \mu^- \mu^-$	5.8×10^{-33}
$\bar{K}^0 \to \pi^+\pi^+ e^- \mu^-$	1.3×10^{-41}

Table 3. The upper limit of Br for 0^-0^- decay channels of D^0.

decay channel	upper limit of Br	Exp. bound on Br [34]	$\frac{s_\Delta h_{ij}}{m^2_\Lambda}$/GeV^{-2}
$D^0 \to \pi^-\pi^- e^+ e^+$	1.8×10^{-29}	$<11.2\times10^{-5}$	<42734
$D^0 \to \pi^-\pi^- \mu^+ \mu^+$	7.2×10^{-30}	$<2.9\times10^{-5}$	<21080
$D^0 \to \pi^-\pi^- e^+ \mu^+$	4.1×10^{-40}	$<7.9\times10^{-5}$	<25371
$D^0 \to \pi^- K^- e^+ e^+$	7.1×10^{-29}	$<20.6\times10^{-5}$	<29548
$D^0 \to \pi^- K^- \mu^+ \mu^+$	2.7×10^{-29}	$<39.0\times10^{-5}$	<39855
$D^0 \to \pi^- K^- e^+ \mu^+$	1.5×10^{-39}	$<21.8\times10^{-5}$	<21683
$D^0 \to K^- K^- e^+ e^+$	6.1×10^{-30}	$<15.2\times10^{-5}$	<86661
$D^0 \to K^- K^- \mu^+ \mu^+$	2.3×10^{-30}	$<9.4\times10^{-5}$	<67045
$D^0 \to K^- K^- e^+ \mu^+$	1.3×10^{-40}	$<5.7\times10^{-5}$	<38177

Table 4. The upper limit of Br for 0^-1^- and 1^-1^- decay channels of D^0.

decay channel	upper limit of Br	decay channel	upper limit of Br
$D^0 \to \pi^-\rho^- e^+ e^+$	2.8×10^{-30}	$D^0 \to \rho^-\rho^- e^+ e^+$	6.7×10^{-31}
$D^0 \to \pi^-\rho^- \mu^+ \mu^+$	9.9×10^{-31}	$D^0 \to \rho^-\rho^- \mu^+ \mu^+$	1.3×10^{-31}
$D^0 \to \pi^-\rho^- e^+ \mu^+$	5.8×10^{-41}	$D^0 \to \rho^-\rho^- e^+ \mu^+$	9.4×10^{-42}
$D^0 \to \pi^- K^{*-} e^+ e^+$	4.8×10^{-30}	$D^0 \to \rho^- K^{*-} e^+ e^+$	2.1×10^{-30}
$D^0 \to \pi^- K^{*-} \mu^+ \mu^+$	1.6×10^{-30}	$D^0 \to \rho^- K^{*-} e^+ \mu^+$	1.2×10^{-41}
$D^0 \to \pi^- K^{*-} e^+ \mu^+$	9.5×10^{-41}	$D^0 \to K^- K^{*-} e^+ e^+$	9.4×10^{-32}
$D^0 \to \rho^- K^- e^+ e^+$	1.4×10^{-29}	$D^0 \to K^- K^{*-} \mu^+ \mu^+$	2.2×10^{-32}
$D^0 \to \rho^- K^- \mu^+ \mu^+$	4.2×10^{-30}	$D^0 \to K^- K^{*-} e^+ \mu^+$	1.5×10^{-42}
$D^0 \to \rho^- K^- e^+ \mu^+$	2.6×10^{-40}	$D^0 \to K^{*-} K^{*-} e^+ e^+$	1.2×10^{-32}

Table 5. The upper limit of Br for 0^-0^- decay channels of $\bar{B}^0$.

decay channel	upper limit of Br	decay channel	upper limit of Br
$\bar{B}^0 \to \pi^+\pi^+ e^- e^-$	7.1×10^{-30}	$\bar{B}^0 \to \pi^+ D_s^+ e^- \mu^-$	1.4×10^{-40}
$\bar{B}^0 \to \pi^+\pi^+ \mu^- \mu^-$	2.8×10^{-30}	$\bar{B}^0 \to K^+ D^+ e^- e^-$	5.2×10^{-30}
$\bar{B}^0 \to \pi^+\pi^+ e^- \mu^-$	1.6×10^{-40}	$\bar{B}^0 \to K^+ D^+ \mu^- \mu^-$	2.0×10^{-30}
$\bar{B}^0 \to \pi^+ K^+ e^- e^-$	2.7×10^{-31}	$\bar{B}^0 \to K^+ D^+ e^- \mu^-$	1.2×10^{-40}
$\bar{B}^0 \to \pi^+ K^+ \mu^- \mu^-$	1.1×10^{-31}	$\bar{B}^0 \to D^+ D^+ e^- e^-$	5.3×10^{-30}
$\bar{B}^0 \to \pi^+ K^+ e^- \mu^-$	6.2×10^{-42}	$\bar{B}^0 \to D^+ D^+ \mu^- \mu^-$	2.1×10^{-30}
$\bar{B}^0 \to \pi^+ D^+ e^- e^-$	7.8×10^{-29}	$\bar{B}^0 \to D^+ D^+ e^- \mu^-$	1.2×10^{-40}
$\bar{B}^0 \to \pi^+ D^+ \mu^- \mu^-$	3.0×10^{-29}	$\bar{B}^0 \to D^+ D_s^+ e^- e^-$	7.2×10^{-29}
$\bar{B}^0 \to \pi^+ D^+ e^- \mu^-$	1.7×10^{-39}	$\bar{B}^0 \to D^+ D_s^+ \mu^- \mu^-$	2.9×10^{-29}
$\bar{B}^0 \to \pi^+ D_s^+ e^- e^-$	6.2×10^{-30}	$\bar{B}^0 \to D^+ D_s^+ e^- \mu^-$	1.6×10^{-39}
$\bar{B}^0 \to \pi^+ D_s^+ \mu^- \mu^-$	2.4×10^{-30}		

Table 6. The upper limit of Br for 0^-1^- decay channels of $\bar{B}^0$.

decay channel	upper limit of Br	decay channel	upper limit of Br
$\bar{B}^0\to\pi^+\rho^+e^-e^-$	6.4×10^{-30}	$\bar{B}^0\to\rho^+D_s^+e^-e^-$	3.8×10^{-31}
$\bar{B}^0\to\pi^+\rho^+\mu^-\mu^-$	2.5×10^{-30}	$\bar{B}^0\to\rho^+D_s^+\mu^-\mu^-$	1.5×10^{-31}
$\bar{B}^0\to\pi^+\rho^+e^-\mu^-$	1.5×10^{-40}	$\bar{B}^0\to\rho^+D_s^+e^-\mu^-$	8.7×10^{-42}
$\bar{B}^0\to\pi^+K^{*+}e^-e^-$	5.1×10^{-31}	$\bar{B}^0\to K^+D^{*+}e^-e^-$	4.0×10^{-30}
$\bar{B}^0\to\pi^+K^{*+}\mu^-\mu^-$	2.0×10^{-31}	$\bar{B}^0\to K^+D^{*+}\mu^-\mu^-$	1.6×10^{-30}
$\bar{B}^0\to\pi^+K^{*+}e^-\mu^-$	1.2×10^{-41}	$\bar{B}^0\to K^+D^{*+}e^-\mu^-$	9.0×10^{-41}
$\bar{B}^0\to\rho^+K^+e^-e^-$	1.8×10^{-32}	$\bar{B}^0\to K^{*+}D^+e^-e^-$	6.9×10^{-30}
$\bar{B}^0\to\rho^+K^+\mu^-\mu^-$	7.2×10^{-33}	$\bar{B}^0\to K^{*+}D^+\mu^-\mu^-$	2.7×10^{-30}
$\bar{B}^0\to\rho^+K^+e^-\mu^-$	4.1×10^{-43}	$\bar{B}^0\to K^{*+}D^+e^-\mu^-$	1.5×10^{-40}
$\bar{B}^0\to\pi^+D^{*+}e^-e^-$	4.7×10^{-29}	$\bar{B}^0\to D^+D^{*+}e^-e^-$	4.2×10^{-31}
$\bar{B}^0\to\pi^+D^{*+}\mu^-\mu^-$	1.8×10^{-29}	$\bar{B}^0\to D^+D^{*+}\mu^-\mu^-$	1.6×10^{-31}
$\bar{B}^0\to\pi^+D^{*+}e^-\mu^-$	1.1×10^{-39}	$\bar{B}^0\to D^+D^{*+}e^-\mu^-$	9.2×10^{-42}
$\bar{B}^0\to\rho^+D^+e^-e^-$	1.3×10^{-28}	$\bar{B}^0\to D^+D_s^{*+}e^-e^-$	4.2×10^{-29}
$\bar{B}^0\to\rho^+D^+\mu^-\mu^-$	4.9×10^{-29}	$\bar{B}^0\to D^+D_s^{*+}\mu^-\mu^-$	1.6×10^{-29}
$\bar{B}^0\to\rho^+D^+e^-\mu^-$	2.8×10^{-39}	$\bar{B}^0\to D^+D_s^{*+}e^-\mu^-$	9.1×10^{-40}
$\bar{B}^0\to\pi^+D_s^{*+}e^-e^-$	1.5×10^{-29}	$\bar{B}^0\to D^{*+}D_s^+e^-e^-$	1.9×10^{-29}
$\bar{B}^0\to\pi^+D_s^{*+}\mu^-\mu^-$	6.0×10^{-30}	$\bar{B}^0\to D^{*+}D_s^+\mu^-\mu^-$	7.3×10^{-30}
$\bar{B}^0\to\pi^+D_s^{*+}e^-\mu^-$	3.5×10^{-40}	$\bar{B}^0\to D^{*+}D_s^+e^-\mu^-$	4.2×10^{-40}

Table 7. The upper limit of Br for 1^-1^- decay channels of $\bar{B}^0$.

decay channel	upper limit of Br	decay channel	upper limit of Br
$\bar{B}^0\to\rho^+\rho^+e^-e^-$	1.3×10^{-30}	$\bar{B}^0\to\rho^+D_s^{*+}e^-\mu^-$	2.2×10^{-42}
$\bar{B}^0\to\rho^+\rho^+\mu^-\mu^-$	5.0×10^{-31}	$\bar{B}^0\to K^{*+}D^{*+}e^-e^-$	1.2×10^{-29}
$\bar{B}^0\to\rho^+\rho^+e^-\mu^-$	3.0×10^{-41}	$\bar{B}^0\to K^{*+}D^{*+}\mu^-\mu^-$	4.4×10^{-30}
$\bar{B}^0\to\rho^+K^{*+}e^-e^-$	4.6×10^{-32}	$\bar{B}^0\to K^{*+}D^{*+}e^-\mu^-$	2.6×10^{-40}
$\bar{B}^0\to\rho^+K^{*+}\mu^-\mu^-$	1.7×10^{-32}	$\bar{B}^0\to D^{*+}D^{*+}e^-e^-$	2.0×10^{-29}
$\bar{B}^0\to\rho^+K^{*+}e^-\mu^-$	9.9×10^{-43}	$\bar{B}^0\to D^{*+}D^{*+}\mu^-\mu^-$	7.7×10^{-30}
$\bar{B}^0\to\rho^+D^{*+}e^-e^-$	2.0×10^{-28}	$\bar{B}^0\to D^{*+}D^{*+}e^-\mu^-$	4.6×10^{-40}
$\bar{B}^0\to\rho^+D^{*+}\mu^-\mu^-$	7.6×10^{-29}	$\bar{B}^0\to D^{*+}D_s^{*+}e^-e^-$	2.0×10^{-28}
$\bar{B}^0\to\rho^+D^{*+}e^-\mu^-$	4.6×10^{-39}	$\bar{B}^0\to D^{*+}D_s^{*+}\mu^-\mu^-$	7.8×10^{-29}
$\bar{B}^0\to\rho^+D_s^{*+}e^-e^-$	9.7×10^{-32}	$\bar{B}^0\to D^{*+}D_s^{*+}e^-\mu^-$	4.6×10^{-39}
$\bar{B}^0\to\rho^+D_s^{*+}\mu^-\mu^-$	3.7×10^{-32}		

Table 8. The upper limit of Br for 0^-0^- decay channels of $\bar{B}_s^0$.

decay channel	upper limit of Br	decay channel	upper limit of Br
$\bar{B}_s^0\to\pi^+K^+e^-e^-$	2.5×10^{-31}	$\bar{B}_s^0\to K^+D_s^+e^-\mu^-$	1.8×10^{-40}
$\bar{B}_s^0\to\pi^+K^+\mu^-\mu^-$	9.8×10^{-32}	$\bar{B}_s^0\to K^+D^+e^-e^-$	2.3×10^{-32}
$\bar{B}_s^0\to\pi^+K^+e^-\mu^-$	5.7×10^{-42}	$\bar{B}_s^0\to K^+D^+\mu^-\mu^-$	9.2×10^{-33}
$\bar{B}_s^0\to K^+K^+e^-e^-$	3.2×10^{-32}	$\bar{B}_s^0\to K^+D^+e^-\mu^-$	5.3×10^{-43}
$\bar{B}_s^0\to K^+K^+\mu^-\mu^-$	1.3×10^{-32}	$\bar{B}_s^0\to D^+D_s^+e^-e^-$	2.4×10^{-30}
$\bar{B}_s^0\to K^+K^+e^-\mu^-$	7.3×10^{-43}	$\bar{B}_s^0\to D^+D_s^+\mu^-\mu^-$	9.5×10^{-31}
$\bar{B}_s^0\to\pi^+D_s^+e^-e^-$	5.6×10^{-29}	$\bar{B}_s^0\to D^+D_s^+e^-\mu^-$	5.4×10^{-41}
$\bar{B}_s^0\to\pi^+D_s^+\mu^-\mu^-$	2.2×10^{-29}	$\bar{B}_s^0\to D_s^+D_s^+e^-e^-$	1.3×10^{-28}
$\bar{B}_s^0\to\pi^+D_s^+e^-\mu^-$	1.3×10^{-39}	$\bar{B}_s^0\to D_s^+D_s^+\mu^-\mu^-$	5.2×10^{-29}
$\bar{B}_s^0\to K^+D_s^+e^-e^-$	8.1×10^{-30}	$\bar{B}_s^0\to D_s^+D_s^+e^-\mu^-$	2.9×10^{-39}
$\bar{B}_s^0\to K^+D_s^+\mu^-\mu^-$	3.2×10^{-30}		

Table 9. The upper limit of Br for 0^-1^- decay channels of $\bar{B}_s^0$.

decay channel	upper limit of Br	decay channel	upper limit of Br
$\bar{B}_s^0\to\pi^+K^{*+}e^-e^-$	1.5×10^{-31}	$\bar{B}_s^0\to K^{*+}D_s^+e^-e^-$	3.6×10^{-30}
$\bar{B}_s^0\to\pi^+K^{*+}\mu^-\mu^-$	6.0×10^{-32}	$\bar{B}_s^0\to K^{*+}D_s^+\mu^-\mu^-$	1.4×10^{-30}
$\bar{B}_s^0\to\pi^+K^{*+}e^-\mu^-$	3.5×10^{-42}	$\bar{B}_s^0\to K^{*+}D_s^+e^-\mu^-$	8.0×10^{-41}
$\bar{B}_s^0\to K^+K^{*+}e^-e^-$	1.6×10^{-32}	$\bar{B}_s^0\to K^+D^{*+}e^-e^-$	4.2×10^{-32}
$\bar{B}_s^0\to K^+K^{*+}\mu^-\mu^-$	6.3×10^{-33}	$\bar{B}_s^0\to K^+D^{*+}\mu^-\mu^-$	1.6×10^{-32}
$\bar{B}_s^0\to K^+K^{*+}e^-\mu^-$	3.6×10^{-43}	$\bar{B}_s^0\to K^+D^{*+}e^-\mu^-$	9.5×10^{-43}
$\bar{B}_s^0\to\rho^+K^+e^-e^-$	5.6×10^{-31}	$\bar{B}_s^0\to K^{*+}D^+e^-e^-$	8.4×10^{-33}
$\bar{B}_s^0\to\rho^+K^+\mu^-\mu^-$	2.2×10^{-31}	$\bar{B}_s^0\to K^{*+}D^+\mu^-\mu^-$	3.3×10^{-33}
$\bar{B}_s^0\to\rho^+K^+e^-\mu^-$	1.3×10^{-41}	$\bar{B}_s^0\to K^{*+}D^+e^-\mu^-$	1.9×10^{-43}
$\bar{B}_s^0\to\pi^+D_s^{*+}e^-e^-$	5.1×10^{-29}	$\bar{B}_s^0\to D_s^+D_s^{*+}e^-e^-$	3.4×10^{-30}
$\bar{B}_s^0\to\pi^+D_s^{*+}\mu^-\mu^-$	2.0×10^{-29}	$\bar{B}_s^0\to D_s^+D_s^{*+}\mu^-\mu^-$	1.3×10^{-30}
$\bar{B}_s^0\to\pi^+D_s^{*+}e^-\mu^-$	1.2×10^{-39}	$\bar{B}_s^0\to D_s^+D_s^{*+}e^-\mu^-$	7.5×10^{-41}
$\bar{B}_s^0\to\rho^+D_s^+e^-e^-$	1.0×10^{-28}	$\bar{B}_s^0\to D^+D_s^{*+}e^-e^-$	1.4×10^{-29}
$\bar{B}_s^0\to\rho^+D_s^+\mu^-\mu^-$	4.0×10^{-29}	$\bar{B}_s^0\to D^+D_s^{*+}\mu^-\mu^-$	5.5×10^{-30}
$\bar{B}_s^0\to\rho^+D_s^+e^-\mu^-$	2.3×10^{-39}	$\bar{B}_s^0\to D^+D_s^{*+}e^-\mu^-$	3.2×10^{-40}
$\bar{B}_s^0\to K^+D_s^{*+}e^-e^-$	1.2×10^{-30}	$\bar{B}_s^0\to D^{*+}D_s^+e^-e^-$	1.7×10^{-30}
$\bar{B}_s^0\to K^+D_s^{*+}\mu^-\mu^-$	4.6×10^{-31}	$\bar{B}_s^0\to D^{*+}D_s^+\mu^-\mu^-$	6.7×10^{-31}
$\bar{B}_s^0\to K^+D_s^{*+}e^-\mu^-$	2.7×10^{-41}	$\bar{B}_s^0\to D^{*+}D_s^+e^-\mu^-$	3.8×10^{-41}

Table 10. The upper limit of Br for 1^-1^- decay channels of $\bar{B}_s^0$.

decay channel	upper limit of Br	decay channel	upper limit of Br
$\bar{B}_s^0\to\rho^+K^{*+}e^-e^-$	4.6×10^{-31}	$\bar{B}_s^0\to K^{*+}D_s^{*+}e^-\mu^-$	4.3×10^{-40}
$\bar{B}_s^0\to\rho^+K^{*+}\mu^-\mu^-$	1.8×10^{-31}	$\bar{B}_s^0\to K^{*+}D^{*+}e^-e^-$	6.4×10^{-32}
$\bar{B}_s^0\to\rho^+K^{*+}e^-\mu^-$	1.1×10^{-41}	$\bar{B}_s^0\to K^{*+}D^{*+}\mu^-\mu^-$	2.5×10^{-32}
$\bar{B}_s^0\to K^{*+}K^{*+}e^-e^-$	5.2×10^{-32}	$\bar{B}_s^0\to K^{*+}D^{*+}e^-\mu^-$	1.4×10^{-42}
$\bar{B}_s^0\to K^{*+}K^{*+}\mu^-\mu^-$	1.9×10^{-32}	$\bar{B}_s^0\to D^{*+}D_s^{*+}e^-e^-$	9.4×10^{-30}
$\bar{B}_s^0\to K^{*+}K^{*+}e^-\mu^-$	1.2×10^{-42}	$\bar{B}_s^0\to D^{*+}D_s^{*+}\mu^-\mu^-$	3.6×10^{-30}
$\bar{B}_s^0\to\rho^+D_s^{*+}e^-e^-$	1.7×10^{-28}	$\bar{B}_s^0\to D^{*+}D_s^{*+}e^-\mu^-$	2.1×10^{-40}
$\bar{B}_s^0\to\rho^+D_s^{*+}\mu^-\mu^-$	6.5×10^{-29}	$\bar{B}_s^0\to D_s^{*+}D_s^{*+}e^-e^-$	3.6×10^{-28}
$\bar{B}_s^0\to\rho^+D_s^{*+}e^-\mu^-$	4.0×10^{-39}	$\bar{B}_s^0\to D_s^{*+}D_s^{*+}\mu^-\mu^-$	1.5×10^{-28}
$\bar{B}_s^0\to K^{*+}D_s^{*+}e^-e^-$	1.9×10^{-29}	$\bar{B}_s^0\to D_s^{*+}D_s^{*+}e^-\mu^-$	8.3×10^{-39}
$\bar{B}_s^0\to K^{*+}D_s^{*+}\mu^-\mu^-$	7.2×10^{-30}		

4 Conclusions

In this paper, we studied the lepton number violation in four-body decays of neutral flavored mesons, including $\bar{K}^0$, D^0, $\bar{B}^0$, and $\bar{B}_s^0$. They are assumed to be induced by a doubly-charged scalar. For $\bar{K}^0$, the channel $\bar{K}^0\to\pi^+\pi^+e^-e^-$ has the largest branching ratio, of the order of 10^{-30}. For D^0, the channel $D^0\to\pi^-K^-l_1^+l_2^+$ has the largest order of magnitude of 10^{-29}. By comparing with the E791 experimental data, we find the upper limit for $\frac{s_\Delta h_{ij}}{m_\Delta^2}$ of the order of 10^4 GeV^{-2}. For $\bar{B}^0$ and $\bar{B}_s^0$, the largest values of the branching ratio is also about 10^{-28}. As these values are extremely small, there are no prospects for detection of such processes in the near future. However, the constraints for such channels may provide guidance for the studies of neutrino-less double beta decays of mesons. We expect more experimental data for such processes from the LHCb and Belle-II Collaborations.

Appendix A

Wave functions of mesons

With the instantaneous approximation, the Bethe-Salpeter wave function of the meson fulfills the full Salpeter equations [36]

$$\begin{aligned}&(M-\omega_1-\omega_2)\varphi_P^{++}(q_\perp)=\Lambda_1^+\eta_P(q_\perp)\Lambda_2^+,\\&(M+\omega_1+\omega_2)\varphi_P^{--}(q_\perp)=-\Lambda_1^-\eta_P(q_\perp)\Lambda_2^-,\\&\varphi_P^{+-}(q_\perp)=\varphi_P^{-+}(q_\perp)=0,\end{aligned}\tag{A1}$$

where $q_\perp^\mu = q^\mu - \frac{P\cdot q}{M^2}P^\mu$, $\omega_1 = \sqrt{m_1^2 - q_\perp^2}$, and $\omega_2 = \sqrt{m_2^2 - q_\perp^2}$; m_1 and m_2 are the masses of quarks and antiquarks, respectively; $\Lambda_i^\pm = \frac{1}{2\omega_i}\left[\frac{\not P}{M}\omega_i \mp (-1)^i(\not q_\perp + m_i)\right]$ is the projection operator. In the above equation, we have defined

$$\eta_P(q_\perp) = \int \frac{\mathrm{d}^3 k_\perp}{(2\pi)^3} V(P; q_\perp, k_\perp)\varphi_P(k_\perp), \tag{A2}$$

and

$$\varphi_P^{\pm\pm}(q_\perp) = \Lambda_1^\pm \frac{\not P}{M}\varphi_P(q_\perp)\frac{\not P}{M}\Lambda_2^\pm, \tag{A3}$$

where $\varphi_P(q_\perp)$ is the wave function, which is constructed using $\not q_\perp$, $\not P$, and the polarization vector. Here we only show the expression for the positive energy part of the wave function. For the 1^- state, it has the form

$$\begin{aligned}\varphi_{1^-}^{++}(q_\perp) = (q_\perp\cdot\epsilon)\Big[&A_1(q_\perp) + \frac{\not P}{M}A_2(q_\perp) + \frac{\not q_\perp}{M}A_3(q_\perp) \\ &+ \frac{\not P \not q_\perp}{M^2}A_4(q_\perp)\Big] + M\not\epsilon\Big[A_5(q_\perp) + \frac{\not P}{M}A_6(q_\perp) \\ &+ \frac{\not q_\perp}{M}A_7(q_\perp) + \frac{\not P \not q_\perp}{M^2}A_8(q_\perp)\Big].\end{aligned} \tag{A4}$$

For the 0^- state, it has the form

$$\varphi_{0^-}^{++}(q_\perp) = \left[B_1(q_\perp) + \frac{\not P}{M}B_2(q_\perp) + \frac{\not q_\perp}{M}B_3(q_\perp) + \frac{\not P \not q_\perp}{M^2}B_4(q_\perp)\right]\gamma_5. \tag{A5}$$

A_i and B_i are functions of $q_\perp^2$, whose numerical values are obtained by solving Eq. (A1).

The interaction potential used in this work has the form [36]

$$V(\vec{q}) = V_s(\vec{q}) + \gamma_0 \otimes \gamma^0 V_v(\vec{q}), \tag{A6}$$

where

$$\begin{aligned}V_s(\vec{q}) &= -\left(\frac{\lambda}{\alpha} + V_0\right)\delta^3(\vec{q}) + \frac{\lambda}{\pi^2}\frac{1}{(\vec{q}^2+\alpha^2)^2}, \\ V_v(\vec{q}) &= -\frac{2}{3\pi^2}\frac{\alpha_s(\vec{q})}{\vec{q}^2+\alpha^2}, \\ \alpha_s(\vec{q}) &= \frac{12\pi}{27}\frac{1}{\ln\left(a + \frac{\vec{q}^2}{\Lambda_{QCD}^2}\right)}.\end{aligned} \tag{A7}$$

The parameters involved are $a = e = 2.71828$, $\alpha = 0.06$ GeV, $\lambda = 0.21$ GeV^2, $\Lambda_{\rm QCD} = 0.27$ GeV; V_0 is obtained by fitting the mass of the ground state. The constituent quark masses used are $m_b = 4.96$ GeV, $m_c = 1.62$ GeV, $m_s = 0.5$ GeV, $m_u = 0.305$ GeV, and $m_d = 0.311$ GeV.

References

1 T. Wang, Y. Jiang, Z.-H. Wang, and G.-L. Wang, Phys. Rev. D, **97**: 115031 (2018)
2 M. Magg and C. Wetterich, Phys. Lett. B, **94**: 61 (1980)
3 G. Lazarides, Q. Shafi, and C. Wetterich, Nucl. Phys. B, **181**: 287 (1981)
4 R. N. Mohapatra and G. Senjanovic, Phys. Rev. D**23**: 165 (1981)
5 T. P. Cheng and L. F. Li, Phys. Rev. D, **22**: 2860 (1980)
6 J. C. Pati and A. Salam, Phys. Rev. D, **10**: 275 (1974); 11: 703(E) (1975)
7 R. N. Mohapatra and J. C. Pati, Phys. Rev. D, **11**: 566 (1975)
8 G. Senjanovic and R. N. Mohapatra, Phys. Rev. D, **12**: 1502 (1975)
9 N. Arkani-Hamed, A. G. Cohen, E. Katz, A. E. Nelson, T. Gregoire, and J. G. Wacker, JHEP, **08**: 021 (2002)
10 H. Georgi and M. Machacek, Nucl. Phys. B, **262**: 463 (1985)
11 N. Quintero, Phys. Rev. D, **87**: 056005 (2013)
12 Y.-L. Ma, Phys. Rev. D, **79**: 033014 (2009)
13 G. Bambhaniya, J. Chakrabortty, and S. K. Dagaonkar, Phys. Rev. D, **91**: 055020 (2015)
14 J. Chakrabortty, P. Ghosh, S. Mondal, and T. Srivastava, Phys. Rev. D, **93**: 115004 (2016)
15 C. Picciotto, Phys. Rev. D, **56**: 1612 (1997)
16 ATLAS Collaboration, Report No. ATLAS-CONF-2017-053
17 CMS Collaboration, Report No. CMS-PAS-HIG-16-036
18 N. Quintero, Phys. Lett. B, **764**: 60 (2017)
19 H. Yuan, T. Wang, G.-L. Wang, W.-L. Ju, and J.-M. Zhang, JHEP, **1308**: 066 (2013)
20 H. Yuan, T. Wang, Y. Jiang, Q. Li, and G.-L. Wang, J. Phys. G, **45**: 065002 (2018)
21 H.-R. Dong, F. Feng, and H.-B. Li, Chin. Phys. C, **39**: 013101 (2015)
22 G. L. Castro and N. Quintero, Phys. Rev. D, **87**: 077901 (2013)
23 A. Ali, A. V. Borisov, and N. B. Zamorin, Eur. Phys. J. C, **21**: 123 (2001)
24 C. Patrignani et al (Particle Data Group), Chin. Phys. C, **40**: 100001 (2016)
25 P. Ball and R. Zwicky, Phys. Rev. D, **71**: 014029 (2005)
26 G.-L. Wang, Phys. Lett. B, **633**: 492 (2006)
27 X.-J. Chen, H.-F. Fu, C.S. Kim, and G.-L. Wang, J. Phys. G: Nucl. Part. Phys., **39**: 045002 (2012)
28 C.-H. Chang, Y.-Q. Chen, G.-L. Wang, and H.-S. Zong, Phys. Rev. D, **65**: 014017 (2001)
29 M. L. Swartz, Phys. Rev. D, **40**: 1521(1989)
30 V. Rentala, W. Shepherd, and S. Su, Phys. Rev. D, **84**: 035004 (2011)
31 R. Appel, G. S. Atoyan, B. Bassalleck et al, Phys. Rev. Lett., **85**: 2877 (2000)
32 A. Lai et al (NA48 Collaboration), Eur. Phys. J. C, **30**: 33 (2003)
33 E. Abouzaid et al (KTeV Collaboration), Phys. Rev. Lett., **96**: 101801 (2006)
34 E.M. Aitala et al (Fermilab E791 Collaboration), Phys. Rev. Lett., **86**: 3969 (2001)
35 R. Asij et al (LHCb Collaboration), Phys. Rev. D, **85**: 112004 (2012)
36 C. S. Kim and G.-L. Wang, Phys. Lett. B, **584**: 285 (2004)